

Red photoluminescent PMMA nanohybrid films for modifying the spectral distribution of solar radiation inside greenhouses



S.M. El-Bashir ^{a,*}, F.F. Al-Harbi ^b, H. Elburaih ^b, F. Al-Faifi ^a, I.S. Yahia ^{c,**}

^a Department of Physics & Astronomy, Science College, King Saud University, Riyadh, Saudi Arabia

^b Department of Physics, College of Science, Princess Nora Bint Abdulrahman University, Riyadh, Saudi Arabia

^c Department of Physics, Faculty of Science, King Khalid University, P.O. Box 9004, Abha, Saudi Arabia

ARTICLE INFO

Article history:

Received 9 April 2015

Received in revised form

2 July 2015

Accepted 11 July 2015

Available online 29 July 2015

Keywords:

PMMA nanohybrid

Greenhouse photoselective film

Photosynthesis

Red fluorescence

Photostability

ABSTRACT

Luminescent solar concentrator (LSC) films based on Polymethylmethacrylate (PMMA) nanohybrids were prepared using free radical polymerization of MMA incorporated with oxide nanoparticles; SiO₂, ZnO and TiO₂. The effect of nano-oxide type was studied by Fourier transform infrared spectroscopy (FT-IR), UV–Vis absorption and fluorescence spectroscopy measurements. The performance of LSC nanohybrid films was evaluated and optimized for photosensitive greenhouse cladding applications in order to increase the plant productivity by changing the solar spectrum. It was found that ZnO nanohybrid LSC film had offered the best spectral properties for photosynthetic active radiation besides their excellent resistance to photo and thermal degradation especially in hot countries like KSA. Regarding thermal efficiency, the highest infrared (IR) efficiency has been found for silica nanohybrid LSC film, which reached about 83%. This result is promising to improve thermal efficiency in greenhouse claddings in cold regions and thermal covering systems like solar dryers and solar desalination systems.

© 2015 Elsevier Ltd. All rights reserved.

1. Introduction

Polymer nanohybrids prepared by direct incorporation of nanosized inorganic particles into polymer matrices are of high interest since they can exhibit unique physical and chemical properties, which greatly differ from those of their individual components [1]. In particular, the photophysical properties of PMMA nanohybrids have received considerable attention for optoelectronic devices [2], optical coatings [3], contact lenses [4], optical switches [5], optical waveguides [6], nonlinear optical devices [7] and luminescent solar concentrators (LSCs) [8]. The configuration of LSC is illustrated in Fig. 1, it consists of a plate of a transparent material such as PMMA, doped with luminescent species e.g.; organic fluorescent dyes, quantum dots or rare earth complexes [9–11]. Part of the light emitted by the luminescent particles is guided towards solar cells which are connected to the edges of LSC plate. The main benefit for LSC applications is to

replace a large area of expensive solar cells used in PV panels with a low-priced alternative, thus a reduction in both the cost of the module (\$/W) and the solar power produced (\$/kWh) can be achieved. A key advantage of over conventional concentrating systems is that LSCs can collect both direct and diffuse solar radiation, and so tracking of the sun is not necessary [12]. In a previous work, we had evaluated the performance of fluorescent PMMA thin-film LSCs for greenhouse applications [13]. These films absorb the green-yellow range of visible solar spectra (which is not absorbed by chlorophylls) and fluoresce it as red light which is necessary for the photosynthesis process [14]. These films were found to be promising photosensitive claddings to increase the irradiance level for the photosynthesis process in greenhouses. Actually, fluorescent PMMA films behave like glass which provides more direct light to the plant below the greenhouse claddings [15]. In sunny countries like KSA if there were no diffuse light, only the upper portions of the upper leaves would be brightly lighted by sun, and the diffused light reflecting within the greenhouse that provides energy to the lower tiers of plant leaves. Many papers have been presented that diffused light can improve plant growth, compared to direct light [16,17]. The motivation is greater for the diffuse light to reach more parts of the plant than direct light, since diffused light is scattered more homogeneously about the greenhouse. Technically, the plants

* Corresponding author. Department of Physics, Faculty of Science, Benha University, Egypt.

** Corresponding author. Nano-Science & Semiconductor Labs., Physics Department, Faculty of Education, Ain Shams University, Roxy, Cairo, Egypt.

E-mail address: elbashireg@yahoo.com (S.M. El-Bashir).

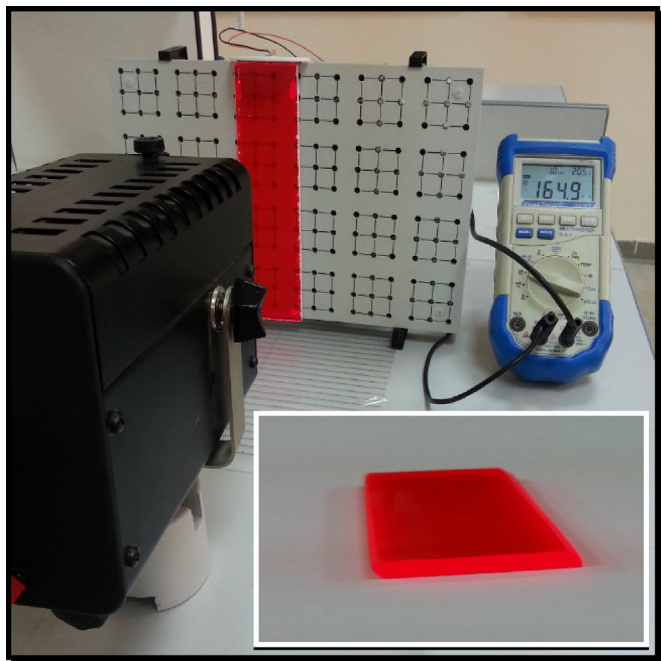


Fig. 1. The device of Luminescent solar concentrator (LSC).

cannot distinguish the difference between direct or diffuse light, each type will cause photosynthesis equally if provided at the same intensity. So, it will be better to provide more diffuse light to plants by using PMMA nanohybrid films based on nanoxide materials incorporated in fluorescent dye doped PMMA. These nanohybrids will generally provide more diffuse light than traditional fluorescent PMMA films due to its translucent nature. In addition, the use of nanotechnology in polymer science have introduced several advantages in different areas such as flammability resistance, optical properties, weathering stability, mechanical strength and antifogging effect [18].

At the present work, a comparative study is made about the effect of three nano-oxide fillers on the photophysical properties and weathering stability of LSC films employed in agriculture applications. The used nano-oxides are SiO₂, ZnO and TiO₂ which are commercially available and largely employed in reflective coatings because of their light scattering properties [19,20]. Rutile phase of TiO₂ was chosen as the most thermodynamically stable and largely employed in the reflective coatings because of its effective light scattering properties [21,22]. A schematic diagram of new nanohybrid LSCs is shown in Fig. 2, they are promising candidates for greenhouse claddings by which the diffuse radiation penetrates deeper into plant canopy for better light distribution, decreased temperature, lowered plant transpiration and subsequently increased photosynthesis and growth [23].

2. Experimental techniques

2.1. Preparation of fluorescent PMMA syrup

Fluorescent PMMA syrup of average molecular weight 1,000,000 g/mol; was prepared as described before [24], using methylmethacrylate (MMA) monomer (Merck, Germany), 0.05 wt% AIBN initiator (Dupont, USA), 200 ppm of fluorescent dye (MACROLEX Fluorescent Red G, Bayer, Germany). The viscosity of the resulting (PMMA-MMA) syrup was determined using a brook field DV-II + viscometer (USA) and was found to be 36 cP.

2.2. Preparation of PMMA nanohybrid LSC films

Three nano-oxide powder materials namely SiO₂, ZnO and TiO₂; were supplied from (Aldrich Inc., USA), the specifications of all the nanofillers used in this study are illustrated in Table 1. The nanofillers were incorporated into fluorescent PMMA syrup in a 1 wt% proportion and stirred at 40 °C for 30 min under sonication to obtain a homogeneous mixture and adequate transparency. Fluorescent PMMA nanohybrid LSC films were prepared by flow coating of the solution on a smooth polyethylene (PE) substrates which are fixed vertically, then the substrate was spun in a centrifuge at 1000 rpm for 10 s to obtain homogeneous film thickness [25]. The polymerization of the residual monomer was completed by keeping substrates in a drying oven at 50 °C for 6 h, after that the films were carefully removed and cut into the desired area. The film thicknesses were determined using Fizeau fringe technique [26] and were found to be of the order of 40 ± 5 μm.

2.3. Photophysical measurements

The absorption spectra of the hybrid films were recorded in the wavelength range (200–800 nm) by a UV–Vis spectrophotometer (UNICAM, Helios Co., Germany). Steady-state fluorescence spectra were recorded in the wavelength range (500–800 nm) using (SHIMADZU RF-5301 PC, Japan) spectrofluorimeter equipped with a temperature regulator. Diffuse reflectance spectra were recorded in the wavelength range (400–800 nm) using diode array spectrophotometer (X-dap, Polytec, Germany). The reflectance cell is designed to make the incident light coming from a xenon lamp source falls perpendicular on the sample under investigation, then the reflected light is collected by optical fibers to be measured by the spectrophotometer. FT-IR absorbance spectra were recorded by FT-IR spectrophotometer (CARY 500 UV-VIS-NIR, USA) in the wavenumber range (1428–769 cm⁻¹) which corresponds to wavelength range (7–13 μm).

2.4. Outdoor testing of greenhouse prototypes

Preliminary assessment for the application of nanohybrid LSC as a photosensitive greenhouse cladding was simply made by painting the optimized fluorescent PMMA/ZnO nanohybrid solution on a flexible transparent PVC sheet of dimensions 30 × 60 cm². The study was performed on soybean cultivar (Giza 21) which is a summer crop, 24 seeds were planted in a panel of dimensions (40 × 20 × 3) cm³. The panel was filled with a sterilized quartz sandy soil and divided into two parts as shown in Fig. 3; The first part is covered by the PVC sheet colored by coating with red fluorescent PMMA/ZnO nanohybrid. The other part contains the control seeds which were covered by a colorless PVC cladding. This mini greenhouse prototype was tested in Riyadh city (KSA, 2014) during September month; all the planted seeds were monitored for ten days so as to examine the plant response to the nanohybrid LSC cladding.

3. Results & discussion

3.1. Photophysical properties and chemisorption effect

Fig. 4 shows the absorption spectra for the prepared PMMA nanohybrid LSC films recorded in the wavelength range (200–800 nm). It is noticed that the first absorption band is appeared in the UV region characterizing π–π* transition in the excited states of carbonyl group of PMMA [27]; the maximum blue shift is observed for SiO₂ and maximum red shift for ZnO nanofiller. This indicates the enhancement of the UV transparency for SiO₂

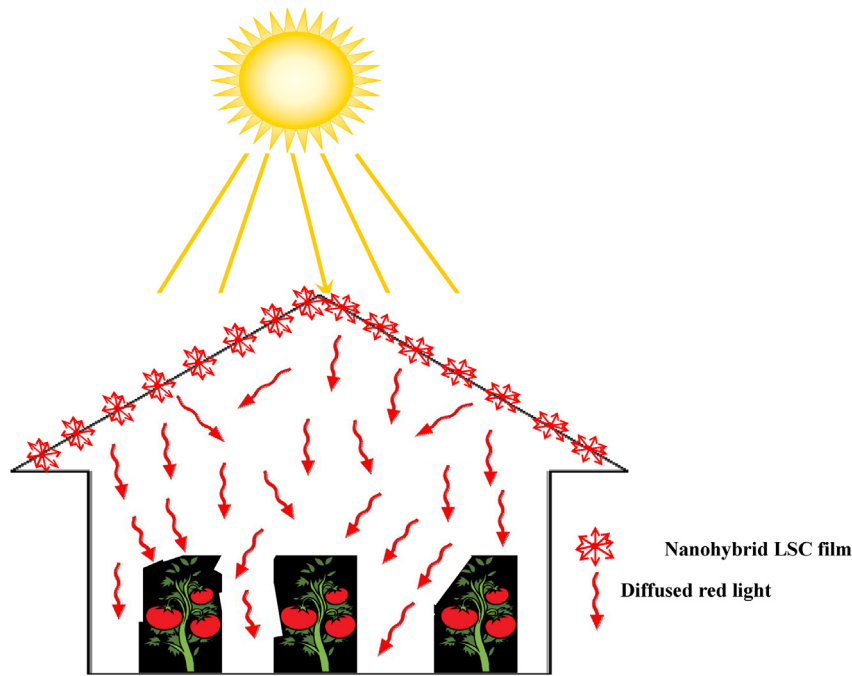


Fig. 2. Uniform light scattering by LSC greenhouse films based on PMMA nanohybrid LSC films.

Table 1

Oxide nanoparticles used in the study; average particle size (APS), specific surface area (SSA).

| Nano-oxide | APS (nm) | Morphology | SSA m ² /g |
|------------------|----------|------------------|-----------------------|
| SiO ₂ | 12 | Spherical | 175–225 |
| ZnO | <100 | Nearly spherical | 15–25 |
| TiO ₂ | <100 | Spherical | 50 |

doped nanohybrids due to the increase of the vibrational modes resulting from the formation of hydrogen bonding between C=O groups of PMMA and surface silanol groups Si–OH in nanosilica. The second absorption band is owed to the electronic transition $S_0 \rightarrow S_1$ of the dye molecules [28], it is observed that the dye absorbance shows a maximum value of ZnO doped nanohybrids. This can be ascribed to strong interaction between the dye molecules and the surface of ZnO nanoparticles compared to other nano-oxide fillers.

The adsorption of dye molecules on the surface of nano-oxide fillers was investigated; the apparent association constant for the formation of surface complex, K_{app} , which can be estimated from the changes in the absorbance intensity of the dye molecule from a Benesi-Hildbrand type equation [29].

$$A_{obs} = (1 - \beta)A_0 - \beta A_c \quad (1)$$

where A_{obs} is the absorbance of dye doped polymer syrup containing different concentrations of nano-oxide filler and β denotes for the degree of association of dye molecule to the nano-oxide surface; A_0 and A_c are the absorbance values of the dye doped polymer syrup and of the (nanofiller-dye) complex. At relatively high nano-oxide filler concentrations $[X]$, β can be equated to $\{K_{app}[X]/(1 + K_{app}[X])\}$, thus equation (1) can be written as [30],

$$\frac{1}{A_{obs} - A} = \frac{1}{A_c - A_0} + \frac{1}{K_{app}(A_c - A_0)[X]} \quad (2)$$

a plot of $1/(A_{obs}-A_0)$ versus $1/[X]$ is shown in Fig. 5, the plot

represents a linear relationship with a slope equal to $1/(K_{app}(A_c - A_0))$ and an intercept equal to $1/(A_c - A_0)$, the values of K_{app} were calculated from the slope and intercept and listed in Table 2. It is clear the highest value of K_{app} has been found for TiO₂ nanofiller due its distinctive properties for the adsorption of dyes to the nanoparticle surface [31]. The spectral distribution of the absorption coefficient α for PMMA nanohybrid LSC films was calculated from the relation [32],

$$\alpha(\lambda) = [2.303 A]/d \quad (3)$$

where A is the absorbance; and d is the film thickness, the increased absorption near the band edge is due to the generation of electron transitions from the valence band to the conduction band. The optical absorption edge has been analyzed by the following relation [33],

$$aE = A(E - E_g)^n \quad (4)$$

where E is the photon energy, A is the edge width parameter representing the film quality, E_g is the band gap and the exponent n is determines the type of the band transition. The parameter n has the values $1/2$ for the direct allowed transition and 2 for the indirect allowed transition. The band gap energy can be determined by plotting a graph between $(aE)^{1/n}$ and E , considering the perfect value of “ n ” that gives the best linear fit of a given data set [34]. The best linear relation was obtained by plotting $(aE)^2$ vs E as depicted by Fig. 6-a; this behavior confirms the existence of the allowed direct transitions in all the investigated films. The values of the direct band gap energy E_{gd} were determined from the intercept the photon energy axis by applying the least square fitting method to ensure the linearity behavior of the obtained curves.

On the other hand, the absorption tails could be interpreted in terms of the Dow-Redfield effect taking the form of Urbach rule as the following equation [32],



(a)



(b)

Fig. 3. (a) The planted soybeans (Giza 21) before being placed in the greenhouse prototype and (b) Outdoor testing of greenhouse prototype; (left) PVC cladding coated with PMMA/ZnO nanohybrid film and (right) uncoated PVC cladding.

$$\alpha(E) = \alpha_0 \exp(E/E_U) \quad (5)$$

where α_0 is a constant and E_U is the width of the tail of the localized states in the band gap. The values of E_U were calculated as the reciprocal gradient of the linear portion of plotting $\ln(\alpha)$ against E as shown in Fig. 6-b. The values of E_{gd} and E_U obtained for all the prepared nanohybrid films are listed in Table 2; it is noted that E_{gd} decreases as K_{app} increases because the dye is typically adsorbed on the surface of all the nano-oxide fillers and acts as an electron donor, injecting electrons from its excited state(s) into the conduction band of the semiconductor under visible light irradiation [35]. The increase of E_U as E_{gd} decreased can be attributed to the increase of the degree of matrix disorder as a result of defect levels which leads to the change of the localized states and causes the internal potential fluctuation in the allowed band gap [36]. This study showed that silica and ZnO fillers increased the band gap of PMMA and consequently the dye stability and efficiency of LSC films [37].

The spectral dependence of the fluorescence spectra were recorded for all PMMA nanohybrid LSC films doped with different nano-oxide fillers and plotted as shown in Fig. 7. As a result of nano-

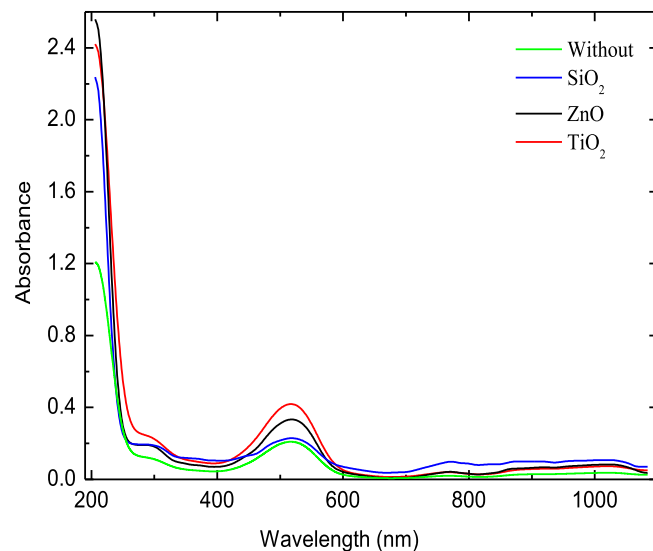


Fig. 4. UV–Vis absorption spectra for PMMA nanohybrid films doped with different nano-oxide fillers.

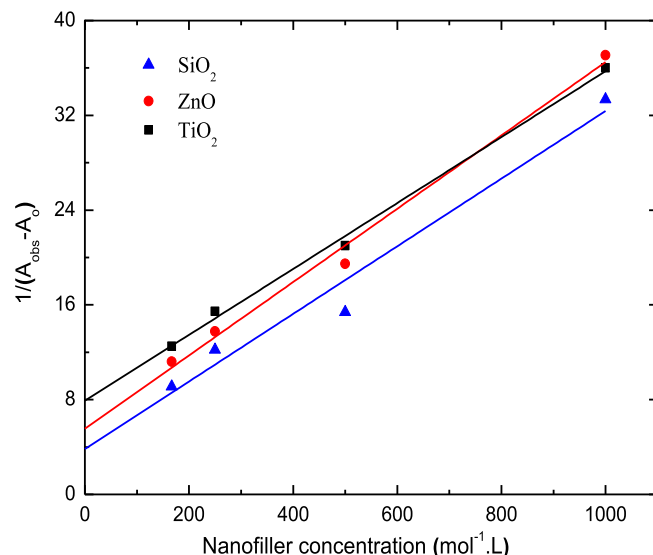


Fig. 5. Benesi–Hildebrand plot for PMMA nanohybrid LSC films doped with different nano-oxide fillers.

Table 2

The photophysical properties of nanohybrid LSC films; the apparent association constant, K_{app} , direct allowed band gap energy, E_{gd} , band tail, E_U , and the fluorescence quantum yield Φ_s .

| Nanofiller | K_{app} ($\text{mol}^{-1}\cdot\text{L}$) | E_{gd} (eV) | E_U (eV) | Φ_s % |
|------------------|--|---------------|------------|------------|
| – | No filler | 5.07 | 0.40 | 23.00 |
| SiO ₂ | 134.00 | 5.32 | 0.29 | 88.70 |
| ZnO | 179.66 | 5.22 | 0.35 | 86.98 |
| TiO ₂ | 284.59 | 5.06 | 0.43 | 65.63 |

oxide doping; it is noted that the fluorescence signal is clearly amplified with a remarkable blue shift in good agreement with our published work [24]. This can be attributed to the chemisorption of the dye molecules on the surface of nano-oxide fillers which lead to the caging of dye molecule on the nano-oxide surface [38]. This unique cage cause the reduction the degree of the translational freedom of the dye molecules and subsequently the intermolecular

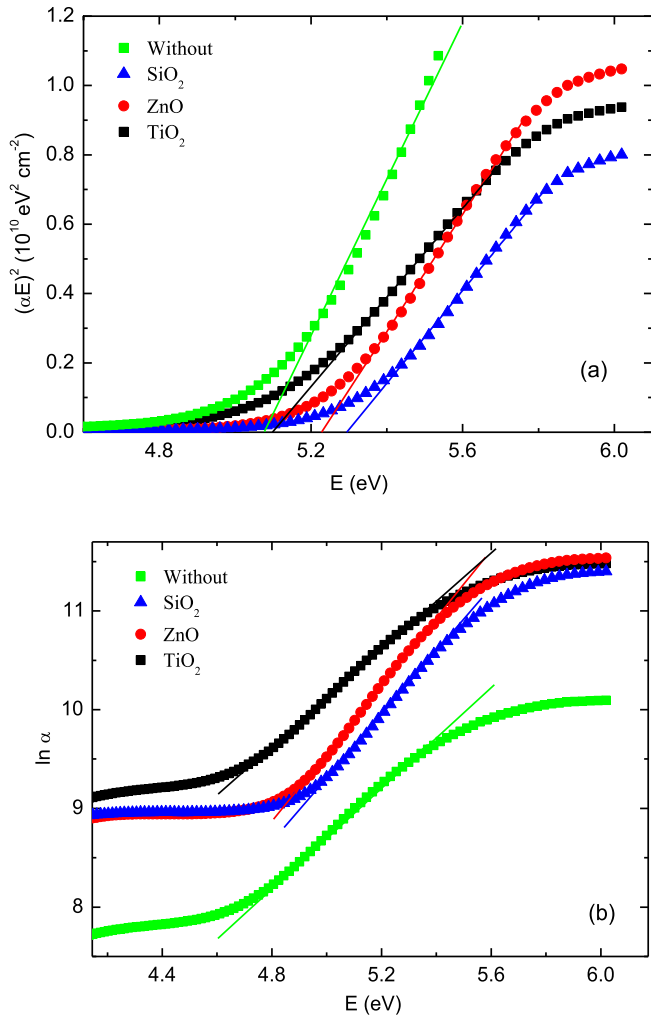


Fig. 6. Interband transitions for the investigated PMMA nanohybrids; the dependence of (a) $(\alpha E)^2$ and (b) $\ln \alpha$ on the photon energy "E".

deactivation processes of fluorescence [39]. Furthermore, the nano-oxide doping contributes significantly to decrease the free volume and chain mobility of PMMA and consequently the internal rotational modes which cause of non-radiative energy losses [40].

The amplification of the fluorescence signal can be explained by calculating the fluorescence quantum yield Φ_s taking Rhodamine 101 as a standard reference ($\Phi_r = 1$ in $H_2O + 0.01\% HCl$) using the following relation [41],

$$\Phi_s = \Phi_r (D_r/D_s)(A_s/A_r)(n_s/n_r) \quad (6)$$

where Φ_r is the fluorescence quantum yield of the standard sample (reference), D_s and D_r are the integrated areas under the corrected fluorescence spectra, A_s and A_r are the optical densities and n_s and n_r are the refractive indices of the tested and reference samples, respectively. The values of Φ_s are presented in Table 2; it is observed that the observed decrease in Φ_s after incorporating of nano-oxide fillers in fluorescent PMMA matrix can be due to the reduction the probability of the formation of dimers (two bonded dye molecules) which are not only weakly fluorescent but also absorb the fluorescence from the monomer (single dye molecule) [42]. The strength of the dye aggregation depends mainly on the host matrix and the factors related to the preparation conditions [43]. This means that the effect Förster-type energy transfer to the excited state dimers (excimers) can be limited by incorporating the dye in a

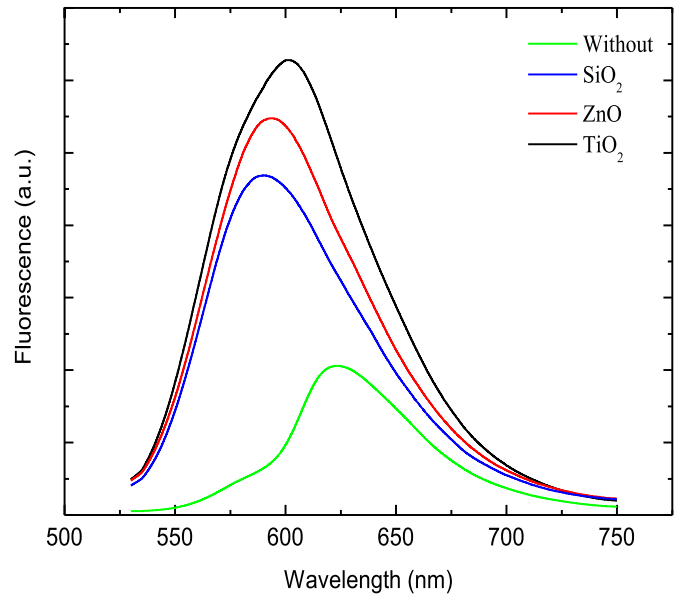


Fig. 7. Fluorescence spectra for PMMA nanohybrid LSC films doped with different nano-oxide fillers.

relatively rigid PMMA nanohybrid matrix than flexible chain PMMA matrix [44].

3.2. Weathering stability tests of nanohybrid LSC films

The long-term photostability of organic fluorescent dyes is one of the most serious difficulties for LSC applications, the photo-response of the investigated LSC nanohybrid films towards natural solar radiation was examined for one year in Riyadh city (KSA 2014). Rectangular samples were placed on an inclined rack which is south faced to sun according to photostability test conditions in the northern hemisphere [45]; so as to ensure the exposure to the full spectrum of solar radiation, from infrared (IR) to ultraviolet (UV) [46]. The photodegradation of dye molecules A_t/A_0 , which is the percentage change of the optical density after sunlight irradiation is plotted against the exposure time as shown in Fig. 8. It is clear that the photodegradation of the dye molecules obeys first order exponential decay based on the following equation [47],

$$A_t/A_0 = C_1 \exp(-Rt) + C_2 \quad (7)$$

where A_t and A_0 are the absorbance values before and after irradiation for a period "t"; C_1 , C_2 are the fitting constants and R is the photodegradation rate constant of the dye molecules. According to the behavior observed in Fig. 8, minor changes in the absorbance were observed after one week of exposure to sunlight; this indicates the stability of the dye molecules which is specialized essentially for plastic coloration [48,49]. The exponential curves showed two degradation steps; the first concerns the dye molecules which may exist outside the free volume of PMMA chains and photo-degrade at a rate constant "R". The second mechanism concerns the dye molecules that exist inside polymer free volume and those chemisorbed on the nano-oxide filler surface and [24]. The values of "R" and C_2 were determined by least square fitting of equation (7) using 1st order exponential decay function as depicted on Fig. 8, and listed in Table 3. It is clear that the addition of nano-oxide fillers enhanced the photostability of nanohybrid LSC films since the photodegradation rate "R" is decreased and the absorbance of the residual amount of dye " C_2 " is increased. This means

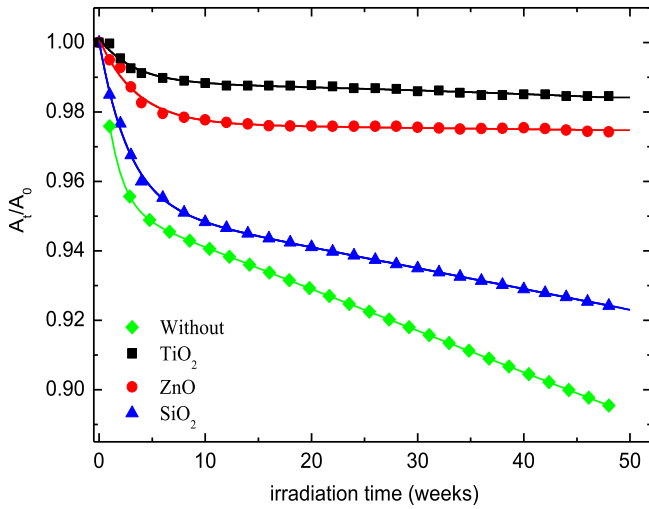


Fig. 8. The photodegradation curves for PMMA nanohybrid LSC films after exposure to daylight for one year (Riyadh, KSA, 2014).

Table 3
The calculated parameters of photo and thermal degradation tests of nanohybrid LSC films for greenhouse cladding applications.

| Nanofiller | $R (10^{-7} s^{-1})$ | $A_t/A_0 \%$ | $E_a (kJ/mol)$ | $I_T/I_0 \%$ |
|------------------|----------------------|--------------|----------------|--------------|
| – | 0.38 | 89.05 | 0.79 | 92.06 |
| SiO ₂ | 10.51 | 92.02 | 4.25 | 78.31 |
| ZnO | 4.76 | 97.82 | 5.57 | 86.92 |
| TiO ₂ | 2.30 | 98.34 | 4.90 | 91.12 |

that LSC matrices based on fluorescent PMMA nanohybrids have long outdoor lifetime compared to those which are only based on PMMA. It was suggested that, introducing of nano-oxide materials in LSCs can be considered as an effective solution for reducing the effect of harmful UV radiation [50]; these materials played a

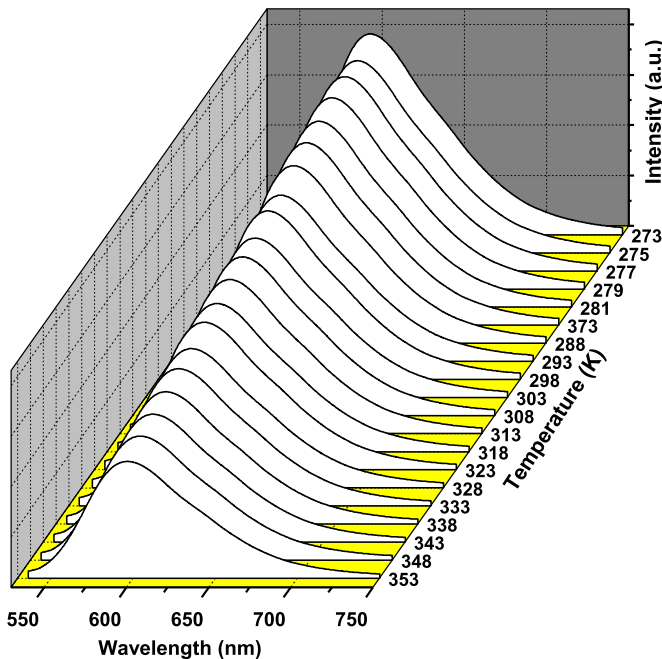


Fig. 9. Temperature dependence of fluorescence intensity for fluorescent PMMA/ZnO LSC film.

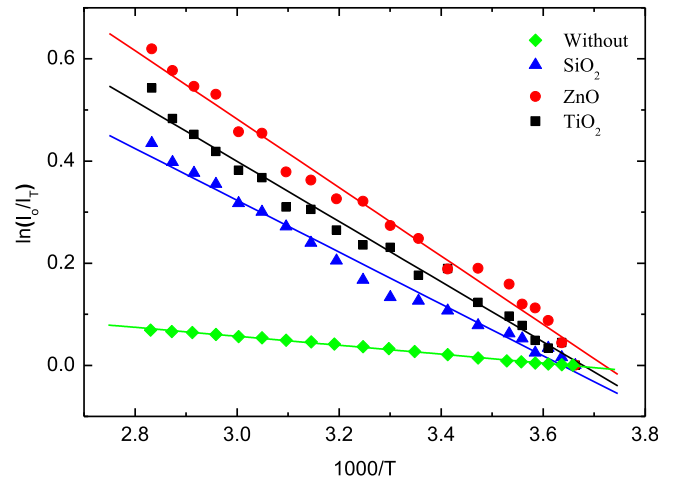


Fig. 10. Arrhenius plot of fluorescence relative intensities, $\ln(I_0/I_T)$ vs. $10^3/T$ for PMMA nanohybrid LSC films.

dominant role on the photodegradation of the dye molecules by causing a perturbation in the number of π electrons and fluorescence deactivation [51].

The effect of temperature on the fluorescence spectra of nanohybrid LSC films was studied in the temperature (0–80 °C); the normalized fluorescence spectra of PMMA/ZnO nanohybrid LSC films is shown in Fig. 9 which represents a typical behavior of all the prepared LSC films. It is observed that as the temperature increases the fluorescence intensity decreases to a value “ I_T ” of its initial value “ I_0 ”. This can be ascribed to the increased phonon assisted relaxation processes; the electronic excitation energy can be dissipated by the vibrational modes existing in the surrounding matrix and the energy levels of the fluorescent species [52]. This means that thermally activated processes for fluorescence deactivation from the excited singlet state can be occurred by varying the temperature of the host medium. This energy transfer occurs at a rate $K_{ET}(T)$, which is plotted in Fig. 10 according to Arrhenius equation [53],

$$K_{ET}(T) = K_{ET}(\infty)\exp(-E_a/RT) \tag{8}$$

where I_0 and I_T are the fluorescence intensities at zero and “ T ” temperatures respectively; “ R ” is the universal gas constant and E_a is the activation energy of the transfer process; Arrhenius plot of $\ln(I_0/I_T)$ versus $10^3/T$ shows a good linear fit for all the prepared LSC films. The calculated values of E_a and I_0/I_T are listed in Table 3; an inspection of these values indicates the improvement in thermal stability of fluorescent dye molecules doped in PMMA nanohybrid matrix than undoped PMMA. After cooling the samples; the fluorescence intensity has been retained to its initial value before heating; the same effect has been happened in the absorption spectra of all the LSC nanohybrid films. This clarifies that there is no major thermal effect on the nanohybrid LSC films which have excellent weathering durability in different climates, since the

Table 4
Spectral properties and efficiency parameters of nanohybrid LSC films for greenhouse cladding applications.

| Nanofiller | $\Delta\lambda_{abs}$ (nm) | $\Delta\lambda_{fluo}$ (nm) | $T_{UVA}\%$ | $T_{Chl}\%$ | $\eta_{abs}\%$ | $\eta_{Red}\%$ | $\eta_{IR}\%$ | $\Delta\eta_{Chl}\%$ |
|------------------|----------------------------|-----------------------------|-------------|-------------|----------------|----------------|---------------|----------------------|
| – | 460–562 | 600–656 | 88.13 | 98.21 | 19.77 | 29.59 | 43.16 | 14.51 |
| SiO ₂ | 480–571 | 558–648 | 87.08 | 96.57 | 46.21 | 88.78 | 82.88 | 45.36 |
| ZnO | 451–582 | 562–638 | 80.40 | 94.05 | 55.71 | 86.62 | 66.93 | 62.15 |
| TiO ₂ | 466–575 | 565–632 | 69.43 | 80.26 | 36.30 | 42.93 | 56.80 | 27.91 |

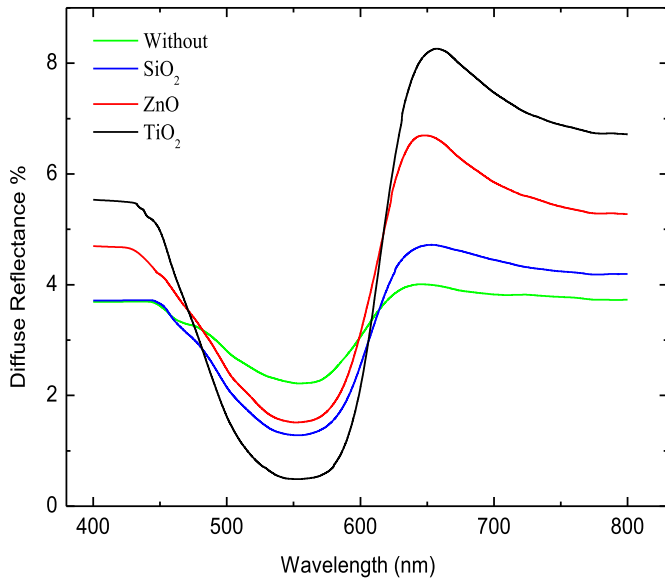


Fig. 11. Diffuse reflectance spectra for PMMA nanohybrid LSC films doped with different nano-oxide fillers.

study had covered a large temperatures range that can be present on the earth surface.

3.3. Improved functionality of nanohybrid LSC films for greenhouse cladding applications

The plant growth response to light depends on specific wavelengths; plants absorb violet and blue bands of the visible spectra and reflect the green color; the maximum sensitivity for photosynthesis lies in the red zone around 660 nm [54]. The spectral characteristics of the visible absorption and fluorescence for nanohybrid LSC films are clarified in Table 4, it is noted that the films have the advantage of absorbing green-yellow light which is not absorbed by chlorophylls and fluoresces it as red light which has a lower energy for the plant growth [55]. The spectral dependence of diffuse reflectance of the nanohybrid LSC films is shown in Fig. 11, it is observed that the photoselective films had a significant peak of reflectivity around 650 nm which is associated with the

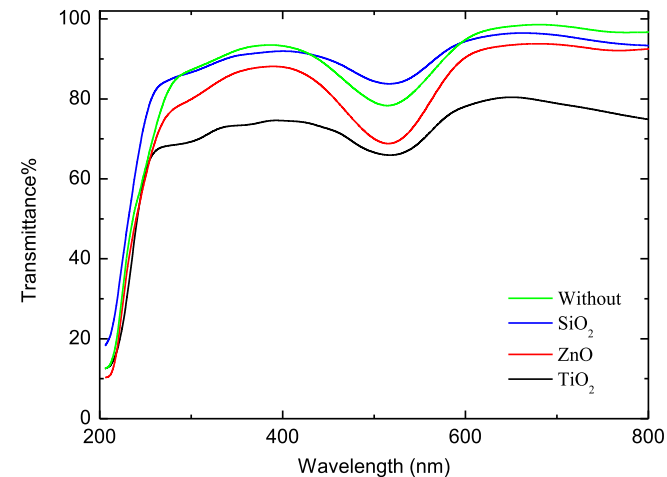


Fig. 12. Transmittance spectra for PMMA nanohybrid LSC films doped with different nano-oxide fillers.

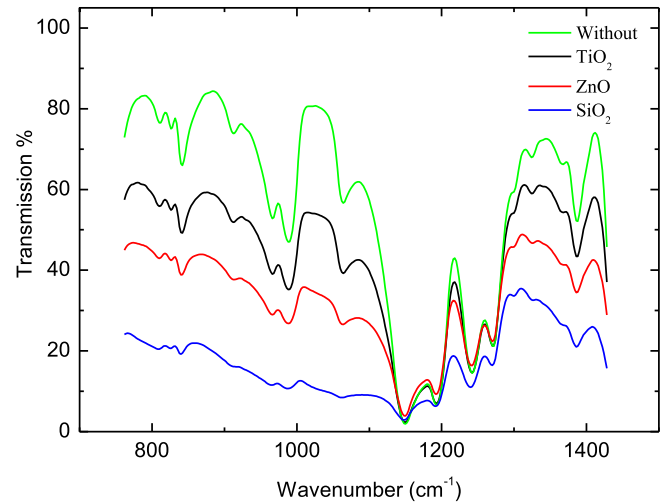


Fig. 13. FT-IR absorption spectra for PMMA nanohybrid LSC films in the 7–13 μm wavelength range.

wavelength absorbed by chlorophylls. This property will introduce a direct influence on plant growth; especially for LSC films doped with ZnO and TiO₂ nanoparticles which can diffuse light more efficiently than the others [56].

Fig. 12 represents the UV–Vis transmittance of the nanohybrid LSC films; from these graphs a remarkable decrease in the transmittance is observed for TiO₂ based nanohybrids in comparison with neat PMMA. This influence is almost negligible for silica and small for ZnO doped nanohybrid LSC films both in visible and UV regions. The values of UVA transmittance T_{UVA} (determined at 320 nm) and chlorophyll transmittance T_{Chl} (determined at 660 nm) are listed in Table 4; most of the prepared LSC films have a high transmission in the visible range. Among all nanoparticles, titanium dioxide offered the maximum reduction of UVA radiation property which in turn caused a considerable visible transmission loss in the titania doped LSC film [57]. In addition, nanosilica incorporation to PMMA matrix yielded an increase of the transmission in the UV–Vis range. Compared to TiO₂ doped

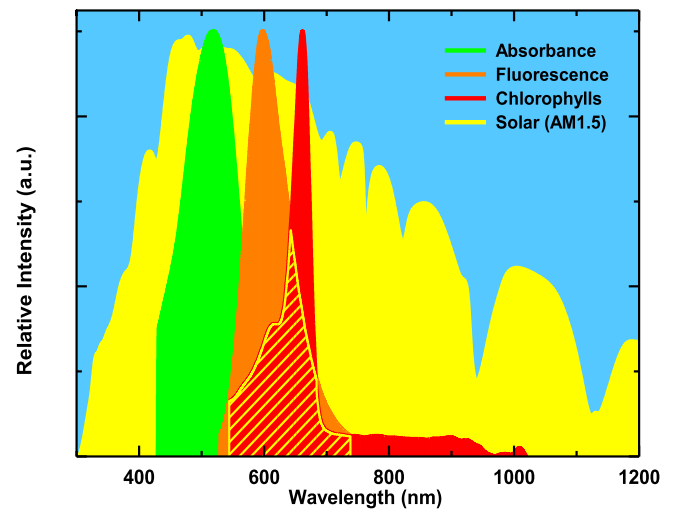


Fig. 14. The absorption and fluorescence spectra for PMMA/ZnO nanohybrid LSC film compared to red absorption spectrum for chlorophylls; the dashed area refers to improved light harvesting for the photosynthesis process (all normalized to AM1.5 solar spectrum).

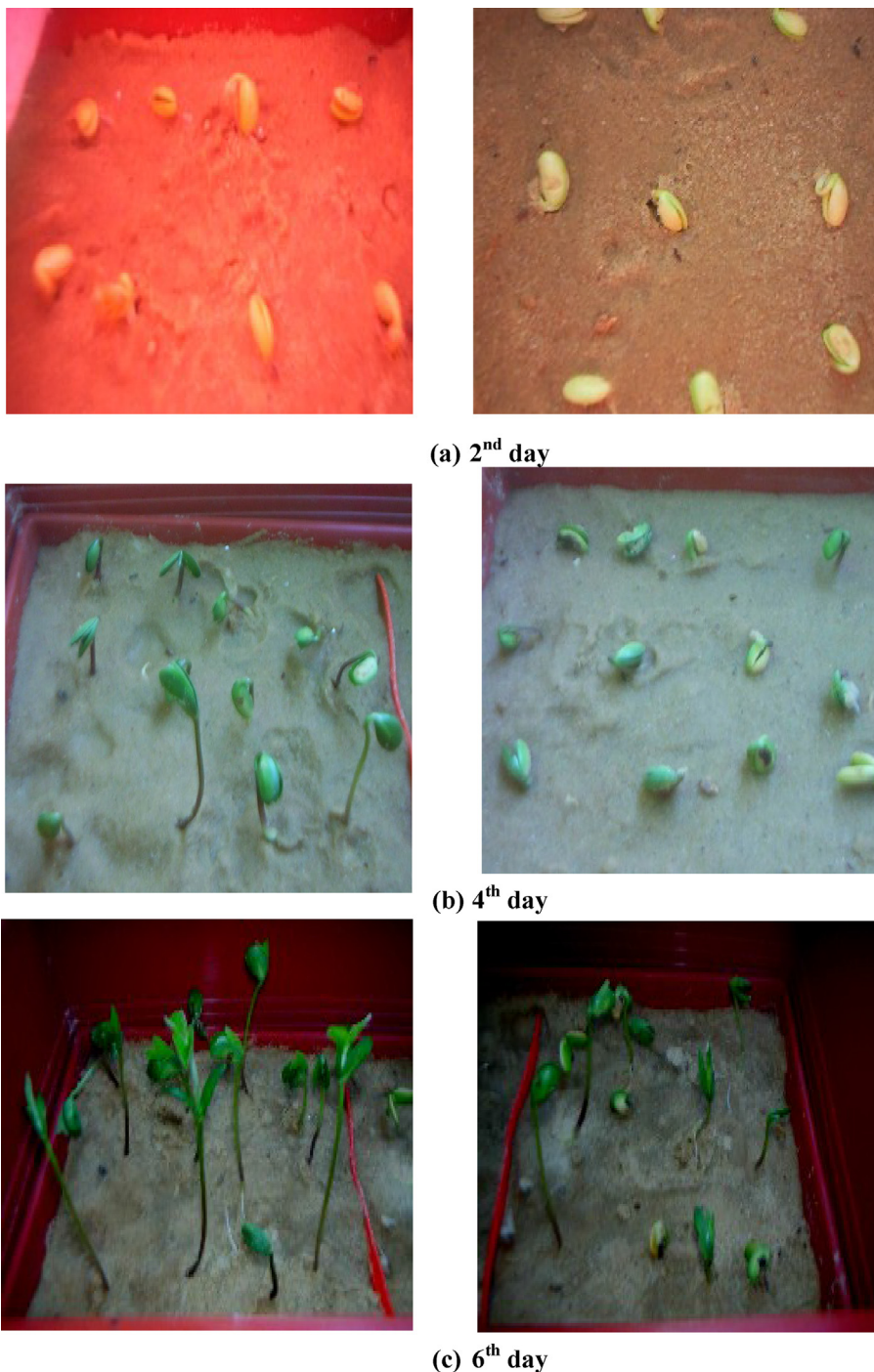


Fig. 15. Growth monitoring for soybeans (Giza 21) planted under the optimized photoselective PMMA/ZnO nanohybrid LSC film; the photographs were taken every two days (September 2014, Riyadh, KSA).

films, ZnO nanocomposites blocked about 20% of UV radiation besides enhanced transmission in the visible range. This means that LSC nanohybrid based on TiO_2 are not suitable for greenhouse covering applications; due to the inherent opacifying nature of titania [58].

3.4. Efficiency parameters of nanohybrid LSC films for greenhouse cladding applications

The absorption efficiency, η_{abs} , defined as the fraction of solar

photons absorbed by LSC film can be calculated as [24],

$$\eta_{abs} = 1 - 10^{-\alpha d} \quad (9)$$

where α is the absorption coefficient at the maximum absorption wavelength and “ d ” is the film thickness; the calculated values of η_{abs} are listed in Table 4 for all the prepared nanohybrid LSC films. It is noted that the value of η_{abs} is significantly increased after adding nano-oxide fillers; reached a maximum value is 55.71% for ZnO doped films. This corroborates the excellent light harvesting by

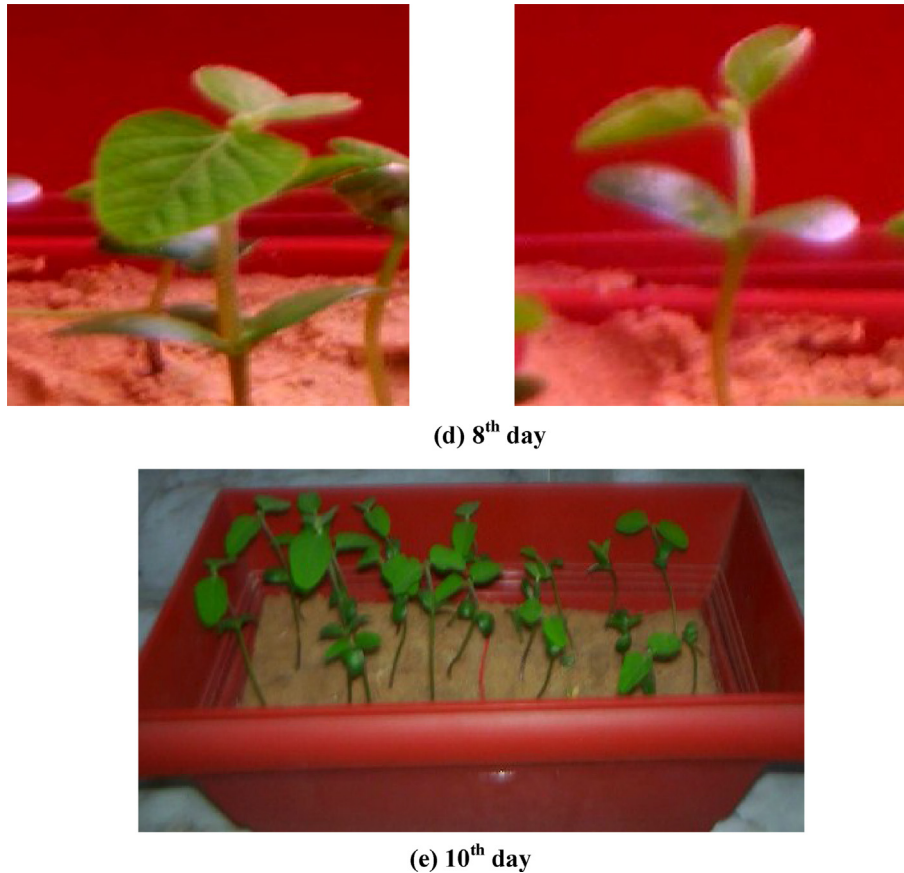


Fig. 15. (continued).

chlorophylls for plants cultivated under photosensitive greenhouse claddings based on ZnO nanohybrid LSC films.

Fig. 13 represents FT-IR spectra of nanohybrid LSC films in the wavelength range (7–13 μm); IR efficiency was calculated as follows [56],

$$\eta_{IR} = [(A_{100} - A_t)/A_{100}] \times 100 \quad (10)$$

where A_{100} is the area under the IR transmission spectrum of a totally transmitting film in the 7–13 μm range, and A_t the area under the spectrum of the tested film; the values of η_{IR} are listed in Table 4. The calculations showed that doping by nano-oxide fillers led to minor increase in IR efficiency indices from 43.16% to 88.70%. In case of titania doped nanohybrid LSCs, efficiency increase was slightly higher. Unlike to films doped with silica nanoparticles presented the highest IR efficiency; this can be attributed to the characteristic IR absorption of nanosilica promoting silica nanohybrids more proper for transparent-thermal covering applications [59].

Fig. 14 shows the action spectrum for photosynthesis in the red band compared to the absorption and fluorescence spectra of the optimized ZnO nanohybrid LSC film. It is noticed that the dye absorbs the green-yellow band which is not utilized by chlorophylls and re-emits it as red light, this means that the high energy of visible solar spectrum can be moved to match the irradiance level for the photosynthesis process.

The enhancement of the total gain of red light obtained by the LSC films is defined by η_{red} , which represents the increase of red band of solar spectrum due to the radiative energy transfer from the absorbed green-yellow band. The value of η_{red} can be evaluated

by the transmitted fluorescence added to the critical cone losses of the fluorescent radiation from a single film side, using the empirical relation [60],

$$\eta_{red} = \left(\Phi_s \times T_{Chl} \times S_a + \frac{1}{2} (1 - R_f) (1 - \eta_{trap}) \right) / S_F \quad (11)$$

where S_a and S_F are the areas of the absorption and fluorescence bands of the FSC photosensitive film normalized to solar spectra, R_f is the Fresnel's reflection coefficient and η_{trap} is the photon trapping efficiency of the host matrix calculated as mentioned in our previous work [8].

The enhancement of photosynthetic active radiation (PAR), $\Delta\eta_{chl}$, which characterizes the enhancement of the total gain of red light in the overlap band between the absorption band of chlorophylls and the fluorescence spectra of the films [60],

$$\Delta\eta_{chl} = (S_{chl}/S_F) \times \eta_{red} \quad (12)$$

S_{chl} is the area of the overlap between the film fluorescence and the action spectrum for photosynthesis in the red band of solar spectrum. The areas S_a , S_F and S_{chl} were calculated from the plot depicted in Fig. 14. The estimated values of η_{red} and $\Delta\eta_{chl}$ in the corresponding wavelength ranges are listed in Table 4 for the investigated nanohybrid LSC films respectively; the highest values are achieved for ZnO based LSC. On the other hand, the lowest values of η_{red} and $\Delta\eta_{chl}$ have been recorded for titania based LSC film. This means that the photosynthesis efficiency in greenhouse is well correlated to fluorescence quantum yield, visible transmission and absorption efficiency of LSC cladding.

3.5. Performance evaluation of greenhouse prototype based on nanohybrid LSC claddings

In the previous discussions, the benefits which can be obtained by nanohybrid LSC films has been demonstrated to have a significant impact on plant growth due to their unique spectral features. ZnO based LSC nanohybrid film has been selected as the optimum photoselective cladding due to its high light harvesting, weathering stability and effective light transmission for photosynthesis. In order to test how the plants can react upon light exposure in greenhouses covered by ZnO based LSC nanohybrid claddings; a prototype of greenhouse has been arranged and evaluated outdoors as illustrated by the image shown in Fig. 3. As illustrated by the image, this mini greenhouse is divided into two parts; the left part is covered by the prepared photoselective LSC cladding and the right is covered by a colorless one (control). Observations on the planted soybean seeds were daily made for ten days; the photographs of the plant growth were taken every 2 day as represented in Fig. 15. On the second day, it is observed that the photoselective LSC cladding transmits a homogeneously red light with a high intensity even under cloudy conditions. The fourth day a significant improvement in the number of growing seedlings has been observed after that, on the sixth day the number of growing leaves is increased with a remarkable improvement in the length and diameter of plant shoots. Finally for the last four days; no significant change was observed between the color of the leaves for the plants under the photoselective LSC and control claddings. Moreover, the plants under photoselective LSC cladding have improved number of buds and increased area of growing leaves. Regarding these observations; it is clear that the plant productivity can be enhanced by photoselective LSC nanohybrid than colorless inert claddings.

4. Conclusions

LSCs films based on PMMA nanohybrids have been prepared and characterized to provide a promising alternative to traditional glass coverings of greenhouses because glass is quite inert, in contrast to polymer, which can easily include low cost fluorescing species which act as green to red light converters of solar spectrum. The incorporation of nano-oxide fillers had offered several advantages for LSCs such as outstanding weathering stability for ZnO and TiO₂ compared to SiO₂ nanoparticles which degraded at a faster rate. In addition, silica nanohybrid LSC was found to attain the highest value of IR efficiency which is not appropriate for greenhouses in hot climates like KSA but advantageous for preserving heat during night time and saving energy for thermal covering systems such as solar dryers and solar desalination systems. Regarding the material efficiency ZnO LSC nanohybrid film acquired the highest (PAR) efficiency parameter ($\Delta\eta_{chl} = 62.15\%$) required for photosynthesis besides outstanding optical properties and photostability. The primary results obtained for soybean seeds planted under ZnO LSC revealed the enhancement of the photosynthetic photon flux (PPF) which is a primary limitation of photoselective claddings [61]. For future considerations, it is necessary to continue our research with photomorphogenesis scientists to elucidate the physiological mechanisms for plant growth and design new LSC photoselective films with specific spectral properties that can meet the various needs of different sectors involved in protected cultivation.

Acknowledgments

This research project was supported by a grant from the Deanship of Scientific Research, Princess Nora Bint Abdul Rahman University (34-K-47).

References

- [1] Y. Oaki, H. Imai, Room-temperature aqueous synthesis of highly luminescent BaWO₄-polymer nanohybrids and their spontaneous conversion to hexagonal WO₃ nanosheets, *Adv. Mater.* 18 (14) (2006) 1807–1811.
- [2] A.H. Yuwono, et al., Controlling the crystallinity and nonlinear optical properties of transparent TiO₂-PMMA nanohybrids, *J. Mater. Chem.* 14 (20) (2004) 2978–2987.
- [3] H. Lu, et al., Fabrication of UV-blocking nanohybrid coating via mini emulsion polymerization, *J. Colloid Interface Sci.* 300 (1) (2006) 111–116.
- [4] G. Ocampo, (2000). U.S. Patent No. 6,030,078. Washington, DC: U.S. Patent and Trademark Office.
- [5] P. Innocenzi, B. Lebeau, Organic-inorganic hybrid materials for non-linear optics, *J. Mater. Chem.* 15 (35–36) (2005) 3821–3831.
- [6] M.M. Demir, et al., Optical properties of composites of PMMA and surface-modified zincite nanoparticles, *Macromolecules* 40 (4) (2007) 1089–1100.
- [7] A.H. Yuwono, et al., Transparent nanohybrids of nanocrystalline TiO₂ in PMMA with unique nonlinear optical behavior, *J. Mater. Chem.* 13 (6) (2003) 1475–1479.
- [8] S.M. El-Bashir, O.A. AlHarbi, M.S. AlSalhi, Thin-film LSCs based on PMMA nanohybrid coatings: device optimization and outdoor performance, *Int. J. Photoenergy* 2013 (2013) 1–10. Article ID 235875.
- [9] M. Debije, Better luminescent solar panels in prospect, *Renew. Energy* 519 (7543) (2015) 298–299.
- [10] M. Fisher, et al., Utilizing vertically aligned CdSe/CdS nanorods within a luminescent solar concentrator, *Appl. Phys. Lett.* 106 (4) (2015). Article ID 041110.
- [11] A.D. Sontakke, et al., Role of electron transfer in Ce³⁺ sensitized Yb³⁺ luminescence in borate glass, *J. Appl. Phys.* 117 (1) (2015). Article ID 013105.
- [12] A.F. Mansour, et al., A qualitative study and field performance for a fluorescent solar collector, *Polym. Test.* 21 (3) (2002) 277–281.
- [13] M. Hammam, et al., Performance evaluation of thin-film solar concentrators for greenhouse applications, *Desalination* 209 (1) (2007) 244–250.
- [14] C. Lamnatou, D. Chemisana, Solar radiation manipulations and their role in greenhouse claddings: Fresnel lenses, NIR- and UV-blocking materials, *Renew. Sustain. Energy Rev.* 18 (2013) 271–287.
- [15] P.J. Sonneveld, G.L.A.M. Swinkels, New developments of energy-saving greenhouses with a high light transmittance, in: *International Conference on Sustainable Greenhouse Systems-greensys2004* 691, 2004, pp. 589–596.
- [16] D.P. Aikman, Potential increase in photosynthetic efficiency from the redistribution of solar radiation in a crop, *J. Exp. Bot.* 40 (8) (1989) 855–864.
- [17] J.G. Pieters, J.M. Deltour, Modelling solar energy input in greenhouses, *Sol. Energy* 67 (1) (1999) 119–130.
- [18] C.C. Chang, F.H. Huang, H.H. Chang, T.M. Don, C.C. Chen, L.P. Cheng, Preparation of water-resistant antifog hard coatings on plastic substrate, *Langmuir* 28 (49) (2012) 17193–17201.
- [19] A.H. Yuwono, et al., Diblock copolymer templated nanohybrid thin films of highly ordered TiO₂ nanoparticle arrays in PMMA matrix, *Chem. Mater.* 18 (25) (2006) 5876–5889.
- [20] S. Li, M.S. Toprak, Y.S. Jo, J. Dobson, D.K. Kim, M. Muhammed, Bulk synthesis of transparent and homogeneous polymeric hybrid materials with ZnO quantum dots and PMMA, *Adv. Mater.* 19 (24) (2007) 4347–4352.
- [21] H. Wang, et al., Single-crystalline rutile TiO₂ hollow spheres: room-temperature synthesis, tailored visible-light-extinction, and effective scattering layer for quantum dot-sensitized solar cells, *J. Am. Chem. Soc.* 133 (47) (2011) 19102–19109.
- [22] K. Zhu, N.R. Neale, A. Miedaner, A.J. Frank, Enhanced charge-collection efficiencies and light scattering in dye-sensitized solar cells using oriented TiO₂ nanotubes arrays, *Nano Lett.* 7 (1) (2007) 69–74.
- [23] D.A. Way, R.W. Pearcy, Sunflecks in trees and forests: from photosynthetic physiology to global change biology, *Tree Physiol.* 32 (9) (2012) 1066–1081.
- [24] M.G. El-Shaarawy, S.M. El-Bashir, M. Hammam, M.K. El-Mansy, Bent fluorescent solar concentrators (BFSCs): spectroscopy, stability and outdoor performance, *Curr. Appl. Phys.* 7 (6) (2007) 643–649.
- [25] S.M. El-Bashir, Photophysical properties of fluorescent PMMA/SiO₂ nanohybrids for solar energy applications, *J. Luminescence* 132 (7) (2012) 1786–1791.
- [26] O.S. Heavens, *Optical Properties of Thin Solid Films*, Courier Corporation, 1991.
- [27] A.F. Mansour, et al., Optical study of perylene dye doped poly (methyl methacrylate) as fluorescent solar collector, *Polym. Int.* 51 (5) (2002) 393–397.
- [28] S.M. El-Bashir, F.M. Barakat, M.S. AlSalhi, Metal-enhanced fluorescence of mixed coumarin dyes by silver and gold nanoparticles: towards plasmonic thin-film luminescent solar concentrator, *J. Luminescence* 143 (2013) 43–49.
- [29] H.A. Benesi, J.H. Hildebrand, A spectrophotometric investigation of the interaction of iodine with aromatic hydrocarbons, *J. Am. Chem. Soc.* 71 (8) (1949) 2703–2707.
- [30] J. He, J. Zhao, T. Shen, H. Hidaka, N. Serpone, Photosensitization of colloidal titania particles by electron injection from an excited organic dye-antennae function, *J. Phys. Chem. B* 101 (44) (1997) 9027–9034.
- [31] D. El Mekki, M.S.A. Abdel-Mottaleb, The interaction and photostability of some xanthenes and selected azo sensitizing dyes with TiO₂ nanoparticles, *Int. J. Photoenergy* 7 (2) (2005) 95–101.

- [32] R.M. Ahmed, S.M. El-Bashir, Structure and physical properties of polymer composite films doped with fullerene nanoparticles, *Int. J. Photoenergy* 2011 (2011) 1–6. Article ID 801409.
- [33] S.M. El-Bashir, F.M. Barakat, M.S. AlSalhi, Double layered plasmonic thin-film luminescent solar concentrators based on polycarbonate supports, *Renew. Energy* 63 (2014) 642–649.
- [34] A.A.M. Farag, I.S. Yahia, Structural, absorption and optical dispersion characteristics of rhodamine B thin films prepared by drop casting technique, *Opt. Commun.* 283 (21) (2010) 4310–4317.
- [35] U. Bach, et al., Solid-state dye-sensitized mesoporous TiO₂ solar cells with high photon-to-electron conversion efficiencies, *Nature* 395 (6702) (1998) 583–585.
- [36] J. Tauc, Optical properties of amorphous semiconductors, in: *Amorphous and Liquid Semiconductors*, Springer Verlag, US, 1974.
- [37] A.F. Mansour, Optical efficiency and optical properties of luminescent solar concentrators, *Polym. Test.* 17 (5) (1998) 333–343.
- [38] D. Avnir, D. Levy, R. Reisfeld, The nature of the silica cage as reflected by spectral changes and enhanced photostability of trapped rhodamine 6G, *J. Phys. Chem.* 88 (24) (1984) 5956–5959.
- [39] R. Reisfeld, Prospects of sol–gel technology towards luminescent materials, *Opt. Mater.* 16 (1) (2001) 1–7.
- [40] C. Sanchez, B. Lebeau, F. Chaput, J.P. Boilot, Optical properties of functional hybrid organic–inorganic nanocomposites, *Adv. Mater.* 15 (23) (2003) 1969–1994.
- [41] G.A. Crosby, J.N. Demas, Measurement of photoluminescence quantum yields. Review, *J. Phys. Chem.* 75 (8) (1971) 991–1024.
- [42] J.R. Lakowicz, *Principles of Fluorescence Spectroscopy*, second ed., Kluwer Academic, Plenum Press, New York, 1999.
- [43] J.C. Pouxviel, B. Dunn, J.I. Zink, Fluorescence study of aluminosilicate sols and gels doped with hydroxy trisulfonated pyrene, *J. Phys. Chem.* 93 (5) (1989) 2134–2139.
- [44] E.T. Knobbe, B. Dunn, P.D. Fuqua, F. Nishida, Laser behavior and photostability characteristics of organic dye doped silicate gel materials, *Appl. Opt.* 29 (18) (1990) 2729–2733.
- [45] T.P. Chang, The Sun's apparent position and the optimal tilt angle of a solar collector in the northern hemisphere, *Sol. Energy* 83 (8) (2009) 1274–1284.
- [46] M.J. Ahmad, G.N. Tiwari, Optimization of tilt angle for solar collector to receive maximum radiation, *Open Renew. Energy J.* 2 (1) (2009) 19–24.
- [47] S.M. El-Bashir, O.A. AlHarbi, M.S. AlSalhi, Optimal design for extending the lifetime of thin film luminescent solar concentrators, *Optik-Int. J. Light Electron Opt.* 125 (18) (2014) 5268–5272.
- [48] T.L. Phillips, J.A. Bodi. (2002). U.S. Patent No. 6,375,864. Washington, DC: U.S. Patent and Trademark Office.
- [49] R.M. Harris, K. Feng, A.R. Burgess. (2000). U.S. Patent No. 6,017,972. Washington, DC: U.S. Patent and Trademark Office.
- [50] Y.H. Zhang, J.H. Xin, W.A. Daoud, X.Y. Hao, UV-blocking properties of silica/titania hybrid nanocomposites, *Key Eng. Mater.* 334 (2007) 1065–1068.
- [51] A.N. Fletcher, *Appl. Phys.* 16 (1) (1978) 93–97.
- [52] M. Sumitani, N. Nakashima, K. Yoshihara, S. Nagakura, Temperature dependence of fluorescence lifetimes of trans-stilbene, *Chem. Phys. Lett.* 51 (1) (1977) 183–185.
- [53] Z.B. Alfassi, R.E. Huie, P. Neta, L.C.T. Shoute, Temperature dependence of the rate constants for reaction of inorganic radicals with organic reductants, *J. Phys. Chem.* 94 (25) (1990) 8800–8805.
- [54] C. Edser, Light manipulating additives extend opportunities for agricultural plastic films, *Plastics Addit. Compd.* 4 (3) (2002) 20–24.
- [55] S.A. Carter, G.B. Alers, M.E. Loik. (2014). U.S. Patent No. 20,140,352,762. Washington, DC: U.S. Patent and Trademark Office.
- [56] C. Espejo, A. Arribas, F. Monzó, P.P. Diez, Nanocomposite films with enhanced radiometric properties for greenhouse covering applications, *J. Plastic Film Sheeting* 28 (4) (2012) 336–350.
- [57] B. Mahltig, H. Böttcher, K. Rauch, U. Dieckmann, R. Nitsche, T. Fritz, Optimized UV protecting coatings by combination of organic and inorganic UV absorbers, *Thin Solid Films* 485 (1) (2005) 108–114.
- [58] A. Verma, S.B. Samanta, N.C. Mehra, A.K. Bakhshi, S.A. Agnihotry, Sol–gel derived nanocrystalline CeO₂–TiO₂ coatings for electrochromic windows, *Sol. Energy Mater. Sol. Cells* 86 (1) (2005) 85–103.
- [59] R. Bhardwaj, M.V. ten Kortenaar, R.F. Mudde, Influence of condensation surface on solar distillation, *Desalination* 326 (2013) 37–45.
- [60] S. El-Bashir, *Photophysical Properties of PMMA Nanohybrids and Their Applications: Luminescent Solar Concentrators & Smart Greenhouses*, LAP LAMBERT Academic Publishing, 2012.
- [61] S.B. Wilson, N.C. Rajapakse, Use of photosensitive plastic films to control growth of three perennial salvias, *J. Appl. Hortic.* 3 (2) (2001) 71–74.